CeO_2-ZrO_2-Al_2O_3 Mixed Oxides for $DeNO_x$ Catalysts

Redox Properties and Catalytic Activity

by Roberta Di Monte, Paolo Fornasiero, Jan Kašpar, Mauro Graziani, Chiara Manfredotti, Gianmario Martra, Salvatore Coluccia, Leonardo Marchese, Paolo Ciambelli, Maria Concetta Gaudino, Diana Sannino, Vladimiro Dal Santo, Rinaldo Psaro and Sandro Recchia

Nanostructured $Ce_mZr_{1-m}O_2$ (m= 0.6, 1) mixed oxides supported on Al_2O_3 were obtained by impregnating γ-Al_2O_3 with cerium/zirconium citrate solutions and subsequent calcination. These materials feature remarkably high surface area stability and oxygen storage after high temperature calcination due to a mutual interaction between the alumina and the supported oxide, which hinders formation of α-alumina. Crucial role of ZrO_2 in preventing the deactivation of the redox capability of CeO_2 due to formation of $CeAlO_3$ is shown. The nano-composite $Ce_{0.6}Zr_{0.4}O_2/Al_2O_3$ mixed oxide was loaded with Pt, characterized and tested under simulated lean $DeNO_x$ conditions.

Ceria-based materials find important applications in applied heterogeneous catalysis [1]. In particular, CeO_2 and more recently CeO_2-ZrO_2 mixed oxides are a key component of the catalytic devices for automotive pollution control [2]. This has led to an intense interest in the properties of these materials in the scientific literature [3-7]. The conversion efficiency of a three-way catalyst (TWC) is strictly related to the so-called oxygen storage/release capacity (OSC), besides other factors. The OSC is the ability to attenuate the negative effects of rich/lean oscillations of exhaust gas composition through the Ce^{4+}/Ce^{3+} redox process. By maintaining a stoichiometric composition at the catalyst, the highest conversion efficiency of the exhaust is attained. Recently, CeO_2-ZrO_2 mixed oxides attracted interest because they are also capable of promoting the activity of silver metal catalysts under simulated lean exhaust conditions [8]. Temperatures as high as 1,273-1,373 K and 1,073-1,173 K can be easily met in the exhausts of respectively conventional- and lean-gasoline engines which requires for high thermal stability of the material. In addition, recent environmental Us Tier 2 regulation [9] required for an urgent improvement of the durability and efficiency of the automotive catalytic converters. Thus, durability as high as 120,000 miles will be phased-in beginning of 2004 in Us. Therefore development of new thermally stable CeO_2-ZrO_2-containing materials is of strong interest in the development of advanced automotive pollution control devices.

In principle, high dispersion and hence activity of CeO_2-based material can be achieved by supporting CeO_2 over a thermally stable support such as alumina [10], however, previous observations [11, 12] and patent claims (see for example Us 5,945,369 issued on August 31st, 1999) clearly indicated the unsuitability of impregnating CeO_2 on Al_2O_3 for production of effective OSC systems. This is due to the fact that the high dispersion and intimate contact of the CeO_2 component with Al_2O_3 may lead upon ageing to formation of $CeAlO_3$ that deactivates the redox properties of the OSC component. Accordingly, it is usual practice to employ pre-formed CeO_2 or CeO_2-ZrO_2 particles to make the TWC. These particles are then supported (wascoated), together with the other components (noble metals and Al_2O_3) on the honeycomb. The pre-

R. Di Monte, P. Fornasiero, J. Kašpar, M. Graziani, Dipartimento di Scienze Chimiche - Università di Trieste - 34127 Trieste; C. Manfredotti, G. Martra, S. Coluccia, Dipartimento di Chimica IFM - Università di Torino - Via P. Giuria, 7 - 10125 Torino; L. Marchese, Dipartimento di Scienze e Tecnologie Avanzate - Università del Piemonte Orientale "A. Avogadro" - C.so Borsalino, 54 - 15100 Alessandria; P. Ciambelli, M.C. Gaudino, D. Sannino, Dipartimento di Ingegneria Chimica ed Alimentare - Università di Salerno - 84084 Fisciano (SA); V. Dal Santo, R. Psaro, Istituto di Scienze e Tecnologie Molecolari - CNR - 20133 Milano; S. Recchia, Dipartimento di Scienze CC FF MM - Università dell'Insubria - 22100 Como. kaspar@univ.trieste.it

sent paper shows that by impregnation of Al_2O_3 with a CeO_2-ZrO_2 component, thermally stable nano-composite materials can be obtained and a key role of ZrO_2 in stabilizing the supported CeO_2 against deactivation is reported.

Experimental

$Ce_mZr_{1-m}O_2$ (13 wt%)/γ-Al_2O_3 (m = 0.6, 1) were prepared by using a modified citrate complexation method [13], by wet impregnating the resulting citrate-containing solution on γ-Al_2O_3 (BET surface area 186 $m^2\ g^{-1}$, pore volume 1.03 ml g^{-1}). Hereafter the samples will be indicated as CZXX/Al_2O_3 where XX indicates the CeO_2 content relative to ZrO_2 (100 or 60 mol%). The preparation of the materials was carried out as follows. $Ce(NO_3)_3 \bullet 6H_2O$ (99.99%, Aldrich) was dissolved in water and mixed with a water solution of $ZrO(NO_3)_2$ (20% ZrO_2, Mel Chemicals), then a water solution of citric acid (99.7%, Prolabo) was added. The ratio metal cation to ligand was 1 to 2.1. The resulting solution was stirred at 348 K for 5 hrs, then at room temperature (rt.) for 12 h, and finally evaporated to carry out an "incipient wetness" impregnation of the support. After impregnation, the materials were dried at 393 K for 12 hrs, heated up to 773 K at a heating rate of 3 K $min.^{-1}$ and then calcined at this temperature for 5 hours to obtain a yellow powder. Hereafter these samples are indicated as fresh ones. Catalysts were aged by calcination at various temperatures (773-1,373 K) for 5, 24 or 48 h. Pt (1.50 wt%) was deposited on the support by incipient wetness technique using $Pt(NH_3)_2(NO_3)_2$ as precursor. A reference Pt/Al_2O_3 (0.88 wt%) sample was also prepared. Temperature programmed reduction (TPR) was carried out in a conventional instrument [14]. Dynamic-OSC was measured by alternately pulsing every 70 s CO (100 µl) and O_2 (100 µl) over the sample (30-100 mg, maintained in a flow of Ar of 25 ml $min.^{-1}$) [14]. Powder XRD spectra were collected on a Siemens Kristalloflex Mod. F Instrument (Ni-filtered CuKα). The peak shape was assumed to be a modified pseudo-Voigt function with asymmetry. Ir spectra were collected on pelletized samples put in a Ir cell attached to a vacuum line, using a Bruker IFS88 spectrophotometer at a resolution of 4 cm^{-1}. Transmission electron micrographs (TEM) were obtained with a Jeol 2000EX microscope. The samples were ultrasonically dispersed in 2-propanol and deposited on a copper grid covered with a lacey carbon film. Catalytic tests were performed with a fixed bed flow micro-reactor, loaded with particles sizing from 180 to 350 µm. Two on-line continuous Ir analyzers for NO, NO_x, C_2H_4, O_2, CO, CO_2 and one on-line gas chromatograph for the analysis of O_2, N_2 and N_2O were used. NO_x-SCR experiments using ethene as reducing agent were carried out in the temperature range of 423-773 K. Steady state values of reactants conversion were measured every 50 K, using an heating rate of 5 K/min. to increase the test temperature. Space velocity was 30,000 h^{-1} (300 mg of sample). Dry feed mixture was composed of 1,000 ppm of NO, 120 ppm of NO_2, 1,000 ppm of C_2H_4, 2.5 vol % of O_2 balance helium, NO_2 concentration being due to the NO-NO_2 equilibrium in the homogeneous phase. Tests in wet condition were performed by adding to the feed mixture 1.3 vol % of water vapor using a saturator at room temperature. Before the catalytic tests all the samples were pretreated in air flow at 773 K. NO_x conversion percentage is defined according to equation (1) whereas N_2O and NO_2 yield percentage, respectively, as in (2) and (3).

$$X_{NOx} = \frac{\left(C^{\circ}_{NOx} - C_{NOx}\right) * 100}{C^{\circ}_{NOx}} \quad (1)$$

$$Y_{N_2O} = \frac{2 * C_{N_2O} * 100}{C^{\circ}_{NO_x}} \quad (2)$$

$$Y_{NO_2} = \frac{C_{NO_2} * 100}{C^{\circ}_{NO_x}} \quad (3)$$

NO_x represents the sum of NO + NO_2, and C_i^o and C_i, respectively, the inlet and outlet reactant concentrations.

Structural and textural characterization of Al_2O_3 and CZ/Al_2O_3 and effects of thermal aging

Table 1 summarizes the structural characterization of Al_2O_3 and $Ce_mZr_{1-m}O_2$/Al_2O_3 samples after calcination in air in the range of temperature of 773-1,373 K.
Calcination progressively transforms γ-Al_2O_3 into θ-Al_2O_3 and α-Al_2O_3, the latter being the only phase detected after 24 h at 1,373 K. In the samples containing also the CZ phase, there is a synergic stabilization between the CZ and Al_2O_3 component, since the transformation process of θ-Al_2O_3 into α-Al_2O_3 is also retarded by the presence of the CZ component. As for the features of the supported CZ phase, after calcination at 1,273 K some phase separation was detected in the case of CZ60/Al_2O_3. This is attributed to some non-homogeneity in the distribution of the CZ precursors over the Al_2O_3 phase induced during the synthesis, rather than phase segregation of the supported $Ce_{0.6}Zr_{0.4}O_2$ phase due to its metastable nature [15]. Consistently, the unsupported $Ce_{0.6}Zr_{0.4}O_2$ made by the similar synthesis method resulted to be a single product (Table). Addition of both Al_2O_3 and ZrO_2 to CeO_2 remarkably hinders the sintering process of the supported CeO_2-containing phase, as indicated by the particle sizes reported in the Table. Thus crystallite size of 77 nm was detected after calcination of CeO_2 at a relatively low temperature (1,173 K), whilst a particle size of 20 nm was detected after calcination at 1,273 K when CeO_2 was supported on Al_2O_3. This value is further reduced when ZrO_2 was introduced into the CeO_2 lattice.
Noticeably, $Ce_{0.6}Zr_{0.4}O_2$ prevents more effectively the Al_2O_3 transformation induced by calcination at 1,373 K compared to CeO_2, which could be related to the smaller particle size of the supported $Ce_{0.6}Zr_{0.4}O_2$ phase, which generates a larger interface with better contact between the two phases and hence stabilization. As a result of this interaction, the surface area of the nano-composite products are thermally stabilized compared to pure Al_2O_3 with respect to thermal ageing. BET surface areas of 12, 32 and 55 $m^2\ g^{-1}$ were measured after calcination at 1,373 K for 24 h respectively for Al_2O_3, CZ100/Al_2O_3 and CZ60/Al_2O_3. This is a remarkable result since such ageing conditions are much more demanding that those routinely employed by industry for laboratory simulations of catalyst deactivation [16]. Addition of CeO_2 [17, 18] or La_2O_3 [19] to γ-Al_2O_3 was shown to hinder the transformation into α-Al_2O_3 presumably by formation of micro-domains of $CeAlO_3$ or $LaAlO_3$ over the alumina surface that may inhibit surface diffusion of species responsible for sintering [19]. However, it should be noted that also ZrO_2 stabilizes alumina

Table - Structural characterization of the catalysts

Sample	Calcination		BET area (m^2g^{-1})	Phase composition (%) Al_2O_3			CZ[a]	CZ Crystallite size (nm)[a]
	Temperature (K)	Time (h)		γ	θ	α		
Al_2O_3	973	5	186	100			-	-
	1,373	5	58		56	44	-	-
	1,373	24	12			100	-	-
$Ce_{0.6}Zr_{0.4}O_2/Al_2O_3$	773	5	180	100			-	
	1,273	5	115		100		c (90) *t* (10)	12 (*c*) 7 (*t*)
	1,373	5	71		100		c (74) *t* (26)	14 (*c*) 7 (*t*)
	1,373	24	55		80	20	*c* (75) *t* (25)	18 (*c*) 10 (*t*)
CeO_2/Al_2O_3	773	5	180	100			-	-
	1,373	5	60		100		*c* (100)	20
	1,373	24	32		34	66	*c* (100)	28
$Ce_{0.6}Zr_{0.4}O_2$	773	5	42	-	-	-	*t"* (100)	5
	1,273	5	<1	-	-	-	*t"* (100)	20
	1,373	5	<1	-	-	-	*c* (85) *t* (15)	20 (*c*) 15 (*t*)
CeO_2	773	5	40	-	-	-	*c* (100)	16
	1,173	5	<1	-	-	-	*c* (100)	77

[a] *Determined by using the Scherrer equation;*

[b] *t" is a tetragonal phase (space group $P4_2/nmc$) with pseudo-cubic cell parameter ratio (c/a) of 1,000; c phase: cubic fluorite type of lattice (space group Fm3m). When a mixture of phases was detected approximate composition were evaluated: c phase: $Ce_{0.8}Zr_{0.2}O_2$; t phase $Ce_{0.2}Zr_{0.8}O_2$.*

[20], suggesting that a more general scenario should be considered.

Summarizing, the results of the textural and structural characterization denote that supporting the CZXX phase (XX= 100 and 60) over Al_2O_3 leads to nano-composite materials featuring remarkably high thermal stability. Negligible effect on thermal stability were observed when Pt was supported on $CZ60/Al_2O_3$ (data not reported).

Dispersion and adsorption properties of the Pt/Al_2O_3 and $Pt/CZ60/Al_2O_3$ phases

The size distribution of the supported Pt particles was examined with TEM microscope and compared with that of the reference Pt/Al_2O_3. Pt/Al_2O_3 calcined at 773 K and subsequently reduced in H_2 at 623 K featured prevalently rounded particles due to a Pt metal phase with a broad distribution of particles sizes ranging from 0.5 to 7.5 nm (Figure 1). The average particle size is 2.5 nm. Elongated Pt metal particles were detected in the $Pt/CZ60/Al_2O_3$ catalyst. Pt particles distribution is largely narrower compared to Pt/Al_2O_3, most of the particles (80%) being within 0.5-1 nm. The average particle size is 1.1 nm. It appears that at equal Pt deposition conditions, the presence of the CZ60 phase favors high Pt dispersion. Formation of a Pt-O-Ce complex was suggested to be responsible for the stabilization of dispersed Pt particles in $Pt/CeO_2/Al_2O_3$ catalysts [21]; formation of a similar complex could also account for the effect of the CZ60 phase on the Pt dispersion found here. Unfortunately, due to fluorescence problems, any attempt to evidence the presence of such a complex by Raman spectroscopy failed.

The adsorption properties were investigated by FtIr spectroscopy using CO as a probe molecule. This widely employed technique allows one to easily detect both dispersion and accessibility of surface Pt sites. For comparison, some measurements were performed also on the metal-free support. For sake of brevity the most relevant results are summarized here. CO adsorption at low temperature on metal-free $CZ60/Al_2O_3$ (spectra not reported) revealed that the $Ce_{0.6}Zr_{0.4}O_2$ is evenly distributed over the Al_2O_3, the overall intensity of the bands associated to CO adsorbed at Al^{3+} coordinatively unsatured sites halving when passing from Al_2O_3 to $CZ60/Al_2O_3$. Moreover, no preferential depletion of residual OH groups that remain on surface Al^{3+} sites after dehydroxylation under the pre-treatment conditions adopted (outgassing at 773 K for 1 h), was observed. These features indicate that the CZ phase is uniformly distributed over the Al_2O_3 surface. The frequencies due to adsorbed CO could be associated with Al^{3+} and Ce^{4+} sites, while no evidence for surface Zr^{4+} sites was found, even though it cannot be fully excluded that the adsorption expected at 2,200 cm^{-1} [22] could be partly masked by bands due CO adsorbed on the Al_2O_3 sites.

The spectra obtained upon CO adsorption at r.t. over Pt/Al_2O_3 and $Pt/CZ60/Al_2O_3$ shown in Figure 2 are in line with the TEM characterization: the intensity of the ν(CO) at 2,062/2,065 cm^{-1} due to CO linearly bonded to surface Pt sites of the metal particles [23] is almost double in the former catalyst. More impor-

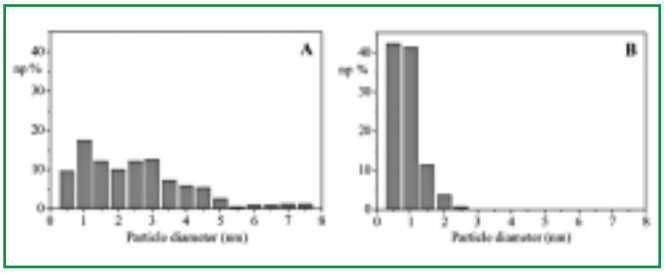

Figure 1 - Particle size distribution detected by TEM on (A) Pt/Al_2O_3 and (B) $Pt/Ce_{0.6}Zr_{0.4}O_2/Al_2O_3$ calcined at 773 K and then reduced (100 torr H_2, 1 h) at 623 K

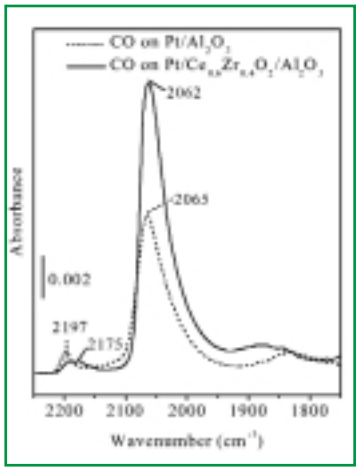

Figure 2 - IR spectra of CO (10 torr) adsorbed at rt. over Pt/Al_2O_3 and $Pt/Ce_{0.6}Zr_{0.4}O_2/Al_2O_3$ calcined at 773 K, reduced in H_2 (100 torr, 1 h) at 623 K and then outgassed at 723 for 1 h

tantly, the relative intensity of the linear (2,065-2,062 cm^{-1}) to bridged CO (1,900-1,800 cm^{-1}) [23] is higher in $Pt/CZ60/Al_2O_3$ compared to Pt/Al_2O_3. Bands attributable to CO adsorbed on the oxide phases are located in the range 2,250-2,170 cm^{-1}: it can be noticed that the intensity of the band at 2,197 cm^{-1} due to CO adsorbed on Al^{3+} with the highest degree of coordinative unsaturation, which are the only ones able to adsorb CO at rt is much lower in $Pt/CZ60/Al_2O_3$, where a band at 2,175 cm^{-1}, associated with CO on Ce^{4+} is formed. In summary, both CO adsorption and TEM results clearly point out that the addition of $Ce_{0.6}Zr_{0.4}O_2$ to Al_2O_3 strongly influences the Pt dispersion, and a high dispersion of Pt particles is favored by this addition. This effect is even more significant when the different Pt loading is taken into account: despite higher loading of Pt in $Pt/CZ60/Al_2O_3$ more dispersed particles are obtained. Further, the $Ce_{0.6}Zr_{0.4}O_2$ appears highly uniformly dispersed over the Al_2O_3 suggesting a strong mutual interaction between the two oxide phases. We believe that this could be at the origin of the high thermal stability above reported.

Redox behavior of the CZ/Al_2O_3 and $Pt/CZ/Al_2O_3$ catalysts

Given the strong interest of the CeO_2-contaning materials in the conventional TWCs catalysts, the redox behavior of $CZ100/Al_2O_3$, $CZ60/Al_2O_3$ and $Pt/CZ60/Al_2O_3$ calcined at 773 K ("fresh" samples") and at 1,273 K was investigated by using the TPR technique (Figure 3). Total-OSC was determined by pulse re-oxidation at 700 K. The reduction profile of $CZ100/Al_2O_3$ calcined at 1,273 K shows three peaks, at ca. 600, 1,000 and 1,200 K, the first two have been attributed to reduction of well dispersed ceria crystallite and bulk ceria, respectively [2, 24]. The third peak has been mainly associated with the reduction of bulk species, leading to formation of $CeAlO_3$. Accordingly, the X-ray diffraction pattern obtained after TPR and a mild oxidation at 700 K (Figure 4, trace B) shows the presence of cerium aluminate. Consistently with the effect of particle size on the reduction profile, the TPR of $CZ100/Al_2O_3$ calcined at 773 K features only broad reduction at relatively low temperatures. $CZ60/Al_2O_3$ calcined at 773 K shows a similar reduction pattern, but, importantly, when the calcination temperature is increased to 1,273 K, the reduction still occurs at relatively low temperature, indicating thermal stabilization of the redox property associated with the addition of ZrO_2. Consistently with the lack of reduction at 1,200 K, no formation of $CeAlO_3$ was detected in the $CZ60/Al_2O_3$ sample (Figure 4, trace C). This indicates that incorporation of ZrO_2 into CeO_2 may prevent this undesirable deactivation pathway.

The lack of formation of the $CeAlO_3$ in the $CZ60/Al_2O_3$ is quite interesting since previous work showed that under similar redox ageing formation at a comparable $Ce_{0.5}Zr_{0.5}O_2$ loading (10 wt%) only a $CeAlO_3$ crystalline phase, in addition to Al_2O_3 could be detected [25]. This result highlights the validity of the simple synthesis methodology here employed in providing efficient redox and thermally stable systems.

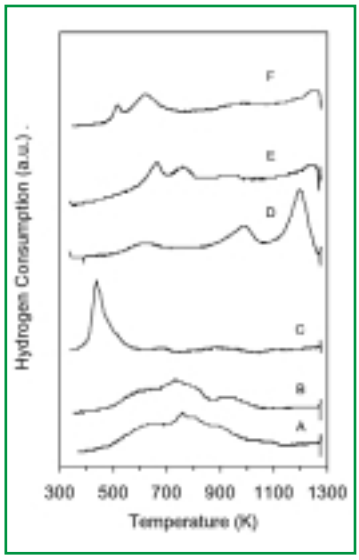

Figure 3 - TPR profiles of (A) CeO_2/Al_2O_3, (B) $Ce_{0.6}Zr_{0.4}O_2/Al_2O_3$ and (C) Pt/ $Ce_{0.6}Zr_{0.4}O_2/Al_2O_3$ calcined at 773 K for 5 h, trace (D) represents the same samples after calcination at 1,273 K

The presence of a homogenous solid solution seems to be a pre-requisite for preventing the deactivation of the CZ/Al_2O_3 system. Accordingly, when the calcination temperature was increased to 1,373 K, where some phase separation into CeO_2-rich and ZrO_2-rich phases occurred, some formation of $CeAlO_3$, induced by the TPR/oxidation at 700 K treatment, was detected by XRD (data not reported).

The presence of Pt shifts all the reduction features to 440 K, in line with the promoting effects of the supported noble metal on the reduction behavior of the CeO_2-ZrO_2 mixed oxides [26]. Generally speaking, it is suggested that spillover phenomena play a key role in the enhanced reduction behavior. H_2 is split at the Pt sites, followed by migration of active hydrogen species over the CZ60 surface favoring its reduction [27], even though other phenomena seem to contribute to these processes [26]. Consistent with the important role of spillover phenomena in the reduction process is the picture obtained after calcination at 1,273 K. All the reduction features shift to somewhat higher temperatures. It is conceivable that the sintering of both CZ60 and Pt phases induced by the high temperature calcination, decreases the extent of the Pt-CZ60 interface thus decreasing the extent of Pt-CZ60 interaction and its capability to promote the reduction at low temperatures. The presence of broad reduction peak above 1,200 K, i.e. at temperatures where formation of $CeAlO_3$ is observed, is consistent with the occurrence of some phase segregation induced by the calcination (compare Table).

Nevertheless, it should be noted that despite this partial deactivation of the TPR behavior, the presence of a CeO_2-ZrO_2 solid solution again appears a crucial factor in conferring high thermal stability to these systems since only high temperature reduction is detected after such aging in the NM-CeO_2 systems (NM = noble metal) [2, 24, 28].

The interaction of H_2 with the Pt loaded catalysts was examined by H_2-TPD (Figure 5) and H_2 chemisorption techniques. $Pt/CZ60/Al_2O_3$ features three desorption peaks centered at 320, 460 and 645 K. The comparison with the TPD profile reported for Pt/Al_2O_3 suggests contribution from H_2 adsorbed on the metal as being responsible for most of the H_2 des-

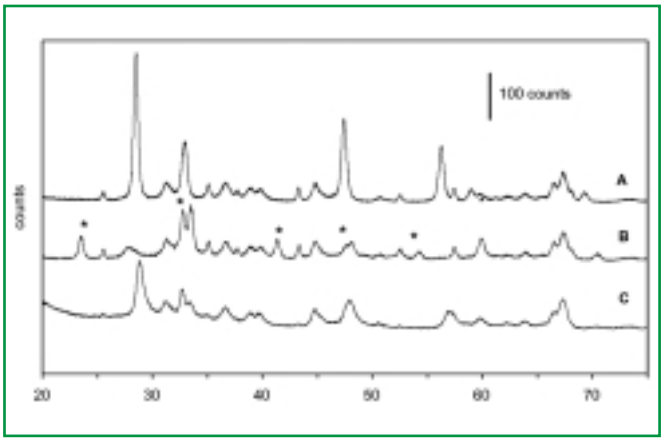

Figure 4 - Powder X-ray diffraction profiles of (A) CeO_2/Al_2O_3 calcined at 1,273 K 5 h, (B) CeO_2/Al_2O_3 calcined at 1,273 K 5 h, subjected to a TPR up to 1,273 K followed by an oxidation at 700 K, and (C) $Ce_{0.6}Zr_{0.4}O_2/Al_2O_3$ calcined 1,273 K 5 h, subjected to a TPR up to 1,273 K followed by an oxidation at 700 K: (*) peaks belonging to $CeAlO_3$

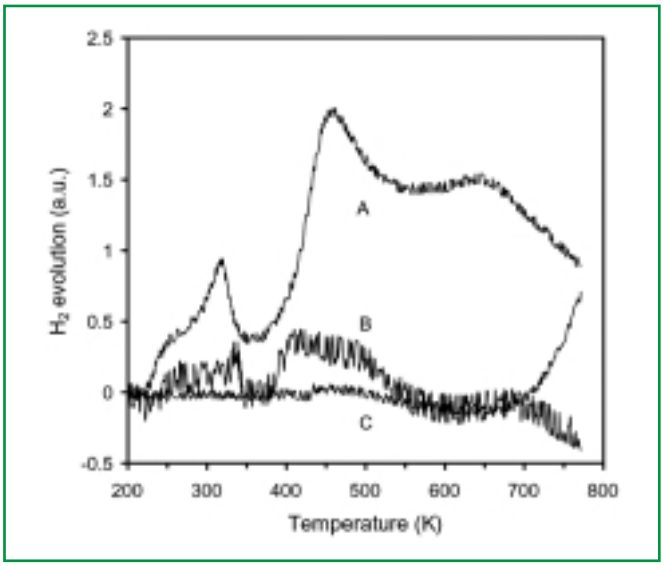

Figure 5 - Temperature programmed desorption of H_2 from (A) $Pt/CZ60/Al_2O_3$, (B) Pt/Al_2O_3, and (C) $CZ60/Al_2O_3$

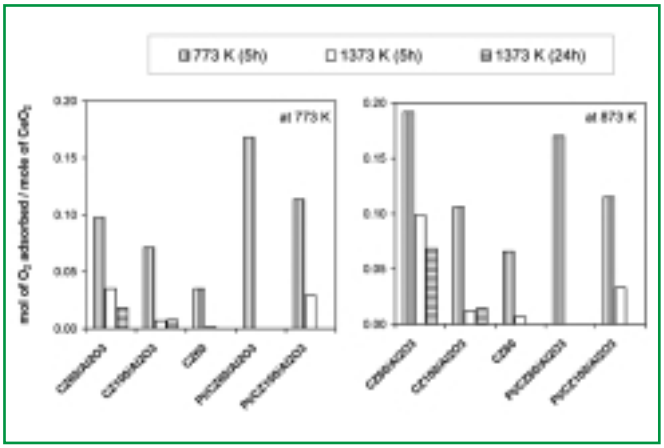

Figure 6 - Dynamic oxygen storage measured at (a) 773 and (b) 873 K over $Ce_{0.6}Zr_{0.4}O_2/Al_2O_3$, CeO_2/Al_2O_3 and $Pt/Ce_{0.6}Zr_{0.4}O_2/Al_2O_3$ samples calcined at 773 and 1,373 K

orbed at low temperatures, even though occurrence of some reverse H_2 spillover cannot be discounted. The effect of interaction between Pt and the $Ce_{0.6}Z_{0.4}O_2$ phase is clearly suggested by the comparison of the desorption pattern obtained for the $CZ60/Al_2O_3$. It is reasonable to associate the H_2 desorption that occurs above 670 K in $CZ60/Al_2O_3$ (Figure 5, C) with the peak at 645 K in the $Pt/CZ60/Al_2O_3$. The presence of the noble metal strongly promotes H_2 storage on the support, which is then reversibly desorbed during the TPD experiment [27]. The presence of spillover phenomena were confirmed by static chemisorption performed at 193 and 298 K. H/Pt = 0.57 and 0.99 were measured respectively at 193 and 298 K over $Pt/CZ60/Al_2O_3$, whilst H/Pt = 0.18 and 0.23 were respectively measured over Pt/Al_2O_3. H_2 chemisorption on the noble metal is a non activated process in contrast to its chemisorption on the support, which is an activated process. The presence of the spillover phenomenon therefore accounts for the increase of the amount H_2 chemisorbed on $Pt/CZ60/Al_2O_3$ with increasing the adsorption temperature, Pt particles being covered with H_2 already at 193 K.

Dynamic OSC was measured using CO as reducing agent. For sake of consistency, all the measured values are reported as mol (O_2) mol $(CeO_2)^{-1}$. As illustrated in Figure 6, the response of the system to the effects of calcination is remarkably different according whether Al_2O_3-supported or unsupported samples are considered.

Negligible OSC was measured over CZ60 after the calcination at 1,373 K, even though significant OSC was measured for this sample in the fresh form (calcined at 773 K). This highlights the crucial role of Al_2O_3 preserving the OSC with respect the effects of high temperature calcination.

It is not clear whether the improvement of the OSC is simply related to the lower particle size of the CZ component in the Al_2O_3 supported samples, e.g. their nano-structured nature, or other effects are operating. In fact, at 773-873 K both surface and bulk of the CeO_2-ZrO_2 mixed oxides may contribute to the CO-OSC [29] suggesting a complex nature of the promoting effect. A perusal of Figure 6 reveals also the crucial role of ZrO_2 in improving the thermal stability of the OSC property. The comparison of the values measured for $CZ60/Al_2O_3$ and $CZ100/Al_2O_3$ after calcination at 1,373 K for 5 and 24 h, respectively, shows that even if the OSC of $CZ60/Al_2O_3$ somewhat declined (which we attribute to the increasing degree of phase separation as detected by XRD), it is always more active compared to the CeO_2/Al_2O_3 system. The deactivation attributed to phase separation is a further points of interest, since it was previously suggested that micro-domain type of mixed oxides might be more efficient as OSC systems compared to single phase solid solution [30]. Addition of Pt clearly promotes the dynamic-OSC at low temperatures, minimizing to some extent the deactivation in the case of $Pt/CZ100/Al_2O_3$. However, the crucial role of added ZrO_2 in enhancing the efficiency of the redox process is again highlighted (in the fresh samples).

Catalytic tests

Catalytic activity of the Pt/Al_2O_3 and $PtCZ60/Al_2O_3$ in the NO_x reduction under simulated lean exhaust was examined in a flow reactor. C_2H_4 was employed as reducing agent.

High activity of $Pt/CZ60/Al_2O_3$ in the presence of water was observed in the range 473-523 K (Figure 7). Ethene was oxi-

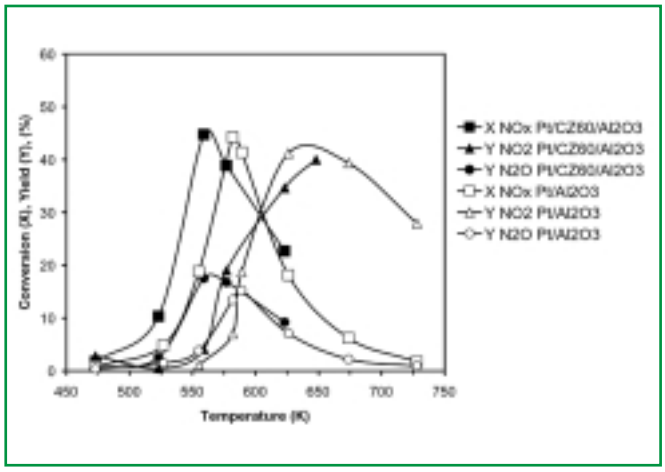

Figure 7 - C_2H_4-DeNO$_x$ results for Pt/Al_2O_3 and $Pt/Ce_{0.6}Zr_{0.4}O_2/Al_2O_3$ catalyst. Feed: 1,000 ppm NO, 120 ppm NO_2, 1,000 ppm C_2H_4, 2.5% O_2, 1.3% H_2O, in He, 30,000 h^{-1}

dized starting from 473 K, reaching 100% of conversion at about 553 K (curve not reported). NO_x conversion showed a maximum in correspondence of total ethene conversion, then decreased. Starting from 523 K, N_2O was produced and a maximum (18%) was observed at 553 K. Due to N_2O formation a maximum N_2 yield of about 27% was obtained. At temperatures above 543 K, production of NO_2 was observed, reaching about 40% at 643 K. At these temperatures, N_2O was still present and NOx conversion was low, below 10%. Comparable performances were evidenced over the Pt/Al_2O_3 catalyst, but the maximum of activity shifted by about 50 K to higher temperatures. Less N_2O production was observed at the maximum (15% at 593 K). Similar NO_2 yield were evidenced above 623 K. In the absence of water (data not reported), comparable results were obtained on both catalysts, except for an higher yield to N_2 (35% at 553 K) on $Pt/CZ60/Al_2O_3$.

The obtained results are in line with the suggested mechanism for the NO_x reduction over Pt catalysts when C_2H_4 is used as reducing agent in that the reaction occurs at the Pt sites, minimizing the effects of the support [31]. Accordingly, the higher Pt dispersion/loading in $Pt/CZ60/Al_2O_3$ with respect to Pt/Al_2O_3 may be indicated as the origin of its higher activity in the lean DeNOx abatement at lower temperature.

Conclusions

The addition of Al_2O_3 to CeO_2-ZrO_2 solid solutions strongly improves the thermal stability of the textural properties and of the redox behavior of the $Ce_{0.6}Zr_{0.4}O_2$ mixed oxide: a strong deactivation of the OSC property did not occurred even after calcination at 1,373 K. The intimate contact between the $Ce_{0.6}Zr_{0.4}O_2$ phase and Al_2O_3 stabilizes high dispersion of the $Ce_{0.6}Zr_{0.4}O_2$ component and, in addition, provides an effective stabilization of the transition aluminas with respect to transformation to the α-Al_2O_3. The crucial role of the presence of the solid solution, i.e. insertion of ZrO_2 into the CeO_2 lattice, was shown to minimize the undesirable reaction of the highly dispersed CeO_2 with Al_2O_3 leading to $CeAlO_3$. The redox behavior is further improved in the presence of Pt particles via a spillover mechanism.

FtIr and TEM investigations indicated a higher dispersion of Pt on the $Ce_{0.6}Zr_{0.4}/Al_2O_3$ support, likely resulting from a stronger interaction between Pt and $Ce_{0.6}Zr_{0.4}O_2$. As a result, the lean DeNOx activity is improved compared to Pt/Al_2O_3.

References

[1] Recent Progress in Catalysis by Ceria and Related Compounds, S. Bernal *et al.* (Eds.), Catal. Today, vol. 50, Elsevier Science, Amsterdam, 1999, 173.
[2] J. Kaspar *et al.,* Ceria-Containing Three Way Catalysts, in Handbook on the Physics and Chemistry of Rare Earths: The Role of Rare Earths in Catalysis, K.A. Gschneidner Jr., L. Eyring (Eds.), Chap.184, Elsevier Science B.V., Amsterdam, 2000, 159.
[3] T. Murota *et al., J. Alloys Comp.,* 1993, **193,** 298.
[4] M. Ozawa *et al., J. Alloys Comp.,* 1993, **193,** 73.
[5] G. Ranga Rao *et al., Catal. Lett.,* 1994, **24,** 107.
[6] A. Trovarelli *et al., J. Catal.,* 1997, 169, 490.
[7] N. Izu *et al., J. Alloys Comp.,* 1998, **270,** 107.
[8] J.N. Hickey *et al., J. Catal.,* in corso di stampa.
[9] Environmental Protection Agency, Federal Register, 2000, **65,** 6697.
[10] A.J. Zarur, J.Y. Ying, *Nature,* 2000, **403,** 65.
[11] J.Z. Shyu *et al., J. Phys. Chem.,* 1988, **92,** 4964.
[12] T. Miki *et al., Chem. Lett.,* 1988, 565.
[13] C. Marcilly *et al., J. Amer. Ceram. Soc.,* 1970, **53,** 56.
[14] N. Hickey *et al., Chem. Commun.,* 2000, 357.
[15] M. Yashima *et al., J. Amer. Ceram. Soc.,* 1994, **77,** 1067.
[16] A. Konig *et al., Topic. Catalysis,* 2001, **16,** 23.
[17] S. Humbert *et al.,* Simultaneous Atmosphere and Temperature Cycling of Three-Way Automotive Exhaust Catalysts, in Catalysis and Automotive Pollution Control III, A. Frennet, J.M. Bastin (Eds.),Elsevier, Amsterdam, 1995, 829.
[18] M.H. Yao *et al., J. Catal.,* 1997, **166,** 67.
[19] F. Oudet *et al., J. Catal.,* 1988, **114,** 112.
[20] T. Horiuchi *et al., Catal. Lett.,* 1999, **62,** 107.
[21] M.S. Brogan *et al., J. Chem. Soc., Faraday Trans.,* 1994, **90,** 1461.
[22] C. Morterra *et al.,* Structural, Morphological and Surface Chemical Features of Al_2O_3 Catalyst Supports Stabilized with CeO_2, in Catalysis and Automotive Pollution Control III, A. Frennet, J.M. Bastin (Eds.), Elsevier, Amsterdam, 1995, 361-373.
[23] N. Sheppard, T. Nguyen, Advances in Infrared and Raman Spectroscopies, R.J.H. Clark, R.E. Hester (Eds.), vol. 5, Heyden, London, 1978, 67.
[24] H.C. Yao, Y.F. Yu Yao, *J. Catal.,* 1984, **86,** 254.
[25] M. Fernandez Garcia *et al., J. Catal.,* 2000, **194,** 385.
[26] P. Fornasiero *et al., J. Catal.,* 1999, **182,** 56.
[27] S. Bernal *et al., J. Catal.,* 1992, **137,** 1.
[28] A. Trovarelli, *Catal. Rev. -Sci. Eng.,* 1996, **38,** 439.
[29] M. Boaro *et al., J. Catal.,* 2000, **193,** 338.
[30] T. Egami *et al., SAE,* 1997, 970461.
[31] R. Burch, T.C. Watling, *Catal. Lett.,* 1997, **43,** 19.

Acknowledgements - The present joint work has been undertaken under the Prin 2000 project “Catalysts for the removal of nitrogen oxides in lean burn engine emissions” which is acknowledged for financial support. Part of this work was also performed within the project “Urban Atmosphere”-Consortium Inca, which is also acknowledged for financial support.